Inorg. Chem. **2007**, *46*, 4905–4916

Origin of the Zero-Field Splitting in Mononuclear Octahedral Dihalide Mn^{II} Complexes: An Investigation by Multifrequency High-Field Electron Paramagnetic Resonance and Density Functional Theory

Carole Duboc,*,† Thida Phoeung,†,‡ Samir Zein,§ Jacques Pécaut,|| Marie-Noëlle Collomb,*,‡ and Frank Neese*,§

Grenoble High Magnetic Field Laboratory, UPR 5021, CNRS, BP 166, 38042 Grenoble Cedex 9, France, Département de Chimie Moléculaire UMR 5250, ICMG FR 2607, CNRS, Université Joseph Fourier, BP 53, 38041 Grenoble Cedex 9, France, Institut für Physikalische und Theoretische Chemie, University of Bonn, Wegelerstrasse 12, 53115 Bonn, Germany, and Laboratoire Coordination et Chiralité, DRFMC-Service de Chimie Inorganique et Biologique, CEA-Grenoble, 38054 Grenoble Cedex 9, France

Received December 13, 2006

The synthesis, structural characterization, and electronic properties of a new series of high-spin six-coordinate dihalide mononuclear Mn^{II} complexes [Mn(tpa)X_2] (tpa = tris-2-picolylamine; X = I (**1**), Br (**2**), and Cl (**3**)) are reported. The analysis of the crystallographic data shows that in all investigated complexes the manganese ion lies in the center of a distorted octahedron with a cis configuration of the halides imposed by the tpa ligand. By a multifrequency high-field electron paramagnetic resonance investigation (95–285 GHz), the electronic properties of **1**–**3** were determined ($D_I = -0.600$, $D_{Br} = -0.360$, $D_{Cl} = +0.115$ cm^{-1}), revealing the important effect of (i) the nature of the halide and (ii) the configuration (cis/trans) of the two halides on the magnitude of *D*. The spin Hamiltonian parameters obtained by density functional theory calculations initiated from the crystal structure of **1**–**3** are in reasonable agreement with the experimental values. The absolute value of *D* is consistently overestimated, but the sign and the trend over the chemical series is well reproduced. Theoretical models (*cis*- and *trans*-[Mn(NH_3)$_4X_2$], X = I, Br, Cl and F) have been used to investigate the different contributions to *D* and also to understand the origin of the experimentally observed changes in *D* within the series reported here. This study reveals that the spin–spin coupling contributions to the ***D*** tensor are non-negligible for the lighter halides (F, Cl) but become insignificant for the heavier halides (I, Br). The four different types of excitations involved in the spin–orbit coupling (SOC) part of the ***D*** tensor contribute with comparable magnitudes and opposing signs. The general trend observed for halide Mn^{II} complexes ($D_I > D_{Br} > D_{Cl}$) can be explained by the fact that the halide SOC dominates the *D* value in these systems with a major contribution arising from interference between metal- and halide-SOC contributions, which are proportional to the product of the SOC constants of Mn and X.

Introduction

Numerous mononuclear manganese(II) complexes have been described in the literature due to their relevance in many scientific domains including biochemistry[1] and catalysis.[2] Studies related to the precise determination of the electronic parameters of such complexes remain rare. Since Mn^{II} is a ^6S state ion with low effective nuclear charge it usually shows neither observable spin-allowed d−d transitions nor intense

* To whom correspondence should be adressed. E-mail: duboc@grenoble.cnrs.fr (C.D.), marie-noelle.collomb@ujf-grenoble.fr (M.-N.C.), neese@thch.uni-bonn.de (F.N.).
† Grenoble High Magnetic Field Laboratory.
‡ Université Joseph Fourier.
§ University of Bonn.
|| CEA-Grenoble.

(1) (a) Bernat, B. A.; Laughlin, L. T.; Armstrong, R. N. *Biochemistry* **1999**, *38*, 7462. (b) Requena, L.; Bornemann, S. *Biochem. J.* **1999**, *343*, 185. (c) Boldt, Y. R.; Whiting, A. K.; Wagner, M. L.; Sadowsky, M. J.; Que, L.; Wackett, L. P. *Biochemistry* **1997**, *36*, 2147. (d) Whittaker, M. M.; Whittaker, J. W. *Biochemistry* **1997**, *36*, 8923. (e) Schwartz, A. L.; Yikilmaz, E.; Vance, C. K.; Vathyam, S.; Koder, R. L.; Miller, A.-F. *J. Inorg. Biochem.* **2000**, *80*, 247. (f) Bogumil, R.; Kappl, R.; Hüttermann, J.; Witzel, H. *Biochemistry* **1997**, *36*, 2345. (g) Smoukov, S. K.; Telser, J.; Bernat, B. A.; Rife, C. L.; Armstrong, R. N.; Hoffman, B. M. *J. Am. Chem. Soc.* **2002**, *124*, 2318.

10.1021/ic062384l CCC: $37.00
Published on Web 05/18/2007

ligand-to-metal charge-transfer transitions that could be used to investigate the electronic structure of such Mn^{II} sites. Thus, the majority of the experimental electronic structure information about Mn^{II} sites derives from magnetic measurements, among which electron paramagnetic resonance (EPR) spectroscopy and related techniques such as electron−nuclear double resonance play a dominant role.[1g,3,] In this respect, the recent progress that has been made in advanced EPR methods, in particular in multifrequency (high-frequency/high-field (HF)) EPR opens up many avenues that lead to detailed electronic structure insights. Specifically, it is now possible to almost routinely investigate Mn^{II} centers by way of a broad range of microwave frequencies (9.4 GHz (X-band), 34 GHz (Q-band), 95 GHz (W-band), and even 285 GHz HF-EPR). HF-EPR allows one for the first time to unambiguously determine the electronic parameters of synthetic[3a−h] and biological[3i−k] mononuclear Mn^{II} complexes to high precision.

As mentioned above, the electronic properties of the high-spin Mn^{II} ion ($3d^5$) in its electronic ground state are characterized by a total electronic spin $S = {}^5/_2$ and a nuclear spin of $I = {}^5/_2$. Since the high-spin d^5 configuration is orbitally nondegenerate, it is well described by a spin Hamiltonian (SH) of the form of eq 1

$$H = \beta \boldsymbol{B}\boldsymbol{g}S + I\boldsymbol{A}S + D[S_z^2 - {}^1/_3S(S+1)] + E(S_x^2 - S_y^2) \quad (1)$$

The two first terms represent the Zeeman and electron nuclear hyperfine interactions, respectively, whereas the last two define the second-order (bilinear) zero-field splitting interaction (ZFS) with D and E being referred to the axial and rhombic parts, respectively. Higher-order ZFS terms in the powers of the fictitious spin S are sometimes included in the analysis of systems with $S > 1$ but in most cases represent small corrections that, furthermore, are difficult to interpret in terms of molecular geometric and electronic structure.

Mononuclear Mn^{II} complexes display a large range of D values ranging from essentially zero (as expected for a Mn^{II} site in a perfectly cubic ligand field) up to 1.21 cm^{-1}.[3] Specifically, for four- or six-coordinate Mn^{II}−dihalide complexes $[Mn(L)_nX_2]$ (X = I, Br and Cl; $n = 4$ for L = pyridine (pyr)[3b,3e] and γ-picoline (pic)[3c] and $n = 2$ for L = N_2H_4,[3a] *o*-phenanthroline (phen),[3c] and $OPPh_3$[3d]), the trend of the magnitude of D is $D_I > D_{Br} > D_{Cl}$ and is proposed to be correlated to the ligand-field strength of the halide ligand ($\Delta_I < \Delta_{Br} < \Delta_{Cl}$). Our recent study of an analogous series of five-coordinate complexes $[Mn(terpy)X_2]$[3f] (terpy = 2,2′:6′,2″-terpyridine) led to the same ordering. Regardless of the coordination number, the magnitude of D is between 0.9 and 1.2 cm^{-1} for the iodo complexes, 0.5 and 0.7 cm^{-1} for the bromo complexes, and 0.16 and 0.30 cm^{-1} for the chloro derivatives,[3a−h] except for the phen series, which is characterized by significantly lower D values ($|D_I| = 0.59$ cm^{-1}, $|D_{Br}| = 0.36$ cm^{-1}, $|D_{Cl}| = 0.12$ cm^{-1}).[3c] It has been suggested that the discrepancy of the phen series originates in the configuration of the halide ligands to the Mn^{II} ion: cis for the phen series and trans for the other six-coordinate complexes (pyr and pic series).

These are highly interesting observations since they provide an, albeit indirect, link between the geometric and electronic structure of the Mn^{II} sites and the coordination geometry as well as covalencies. Many reasons may be responsible for the observed trends: cis versus trans arrangement of the halide ligands, changes in d-orbital splittings with the nature of the halide, changes in π versus σ covalencies, changes in excitation energies, the influence of ligand spin−orbit coupling, or the influence of metal-to-ligand charge-transfer states, to name only a few. In this respect, it is expedient to call on a combined experimental and theoretical investigation in order to determine the nature of the ZFS in Mn^{II} dihalide complexes. Unfortunately, the first-principles theory of the ZFS interaction is still in its infancy and only recently a significant systematic activity has evolved in the quantum chemical community in order to predict the ZFSs of transition-metal complexes using methods based on density functional theory (DFT) or correlated ab initio methods. The present state of knowledge indicates that ligand-field theory (LFT), which is a powerful guide to many properties of transition-metal complexes, is notoriously unreliable for the explanation of ZFSs. While it has been proven possible to fit the ZFSs of countless transition-metal complexes with ligand-field based equations, it may be challenged whether such approaches obtain the right answers for the right reason since the number of disposable parameters that enter the ligand-field based treatments is usually so large that the desired result may readily be obtained. In fact, recent investigations using first-principles quantum chemical methods point to significant contributions from the electron−electron magnetic dipolar spin−spin interaction, something that is almost never taken into account in ligand-field treatments. Furthermore, the crucial role of spin-flip excited states must be recognized.[4] Although they have necessarily been taken into account in the treatment of high-spin d^5 systems, their role is much more

(2) (a) Deroche, A.; Morgenstern-Baradau, I.; Cesario, M.; Guilhem, J.; Keita, B.; Nadjo, L.; Houée-Levin, C. *J. Am. Chem. Soc.* **1996**, *118*, 4567. (b) Shimanovich, R.; Hannah, S.; Lynch, V.; Gerasimchuk, N.; Mody, T. D.; Magda, D.; Sessler, J.; Groves, J. T. *J. Am. Chem. Soc.* **2001**, *123*, 3613. (c) Pan, J. -F.; Chen, K. *J. Mol. Catal. A. Chem.* **2001**, *176*, 19. (d) Wieprecht, T.; Xia, J.; Heinz, U.; Dannacher, J.; Schlingloff, G. *J. Mol. Catal A. Chem.* **2003**, *203*, 113 and references therein.

(3) (a) Birdy, R. B.; Goodgame, M. *Inorg. Chim. Acta* **1981**, *50*, 183. (b) Jacobsen, C. J. H.; Pedersen, E.; Villardsen, J.; Weihe, H. *Inorg. Chem.* **1993**, *32*, 1216. (c) Lynch, W. B.; Boorse, R. S.; Freed, J. H. *J. Am. Chem. Soc.* **1993**, *115*, 10909. (d) Wood, R. M.; Stucker, D. M.; Jones, L. M.; Lynch, W. B.; Misra, S. K.; Freed, J. H. *Inorg. Chem.* **1999**, *38*, 5384. (e) Goodgame, D. M. L.; El Mkami, H.; Smith, G. M.; Zhao, J. P.; McInnes, E. J. L. *Dalton Trans.* **2003**, 34. (f) Mantel, C.; Baffert, C.; Romero, I.; Deronzier, A.; Pécaut, J.; Collomb, M.-N.; Duboc, C. *Inorg. Chem.* **2004**, *43*, 6455. (g) Mantel, C.; Philouze, C.; Collomb M.-N.; Duboc, C. *Eur. J. Inorg. Chem.* **2004**, 3880. (h) Duboc, C.; Astier-Perret, V.; Chen, H.; Pécaut, J.; Crabtree, R. H.; Brudvig, G. W.; Collomb, M.-N. *Inorg. Chim. Acta* **2006**, *359*, 1541. (i) Käss, H.; MacMillan, F.; Ludwig L.; Prisner, T. *J. Phys. Chem. B* **2000**, *104*, 5362. (j) Un, S.; Tabares, L. C.; Cortez, N.; Hiraoka, B. Y.; Yamakura, F. *J. Am. Chem. Soc.* **2004**, *126*, 2720. (k) Kappl, R.; Ranguelova, K.; Koch, B.; Duboc, C.; Hüttermann, J. *Magn. Res. Chem.* **2005**, *43*, S65.

(4) Neese, J. *J. Am. Chem. Soc.* **2006**, *128*, 10213.

universally important, even for configurations such as that of high-spin d^4. The combined effect of spin−spin and spin−orbit contributions to the ZFS makes it a very challenging property to be predicted by quantum chemical methods. It is particularly true in those methods where the total spin does not remain a good quantum number, as is the case for spin-unrestricted DFT treatments. We do not wish to review the entire history of the theory of the ZFS here since this has been done a number of times in the recent past.[5] We merely point to the general formulation of the spin−orbit coupling (SOC) contribution to the ZFS,[6] its approximate realization in a DFT framework,[4,7] where the relation to the DFT treatment of the SOC contribution to the ZFS due to Pederson and Khanna,[7a] as used by several recent authors[4,7,8] is discussed. The spin−spin (SS) contribution to the ZFS in a DFT framework has been initiated by Petrenko et al.[9] and was implemented for large-scale application by several authors recently in various electronic structure variants.[10] Nevertheless, there still is a very limited amount of experience with the application of ZFS theories to transition-metal chemistry, and it is of utmost importance to assess the accuracy and validity of the available approaches on experimentally well-defined systems.

This line of approach defines the main goal of this paper. In particular, we wish to (a) report the synthesis and structural characterization of a new series of six-coordinate mononuclear Mn^{II} complexes of the general formula $[Mn(tpa)X_2]$ (tpa = tris-2-picolylamine; X = I (**1**), Br (**2**), and Cl (**3**)) with a cis configuration of the halide, (b) obtain high-precision experimental data through HF-EPR techniques coupled to computer simulations of the spectra, (c) test the validity of the currently available DFT methods in their application to Mn^{II} sites, and most importantly, (d) understand the origin of the observed ZFS effects in the series of compounds reported. Specifically, we will purposely employ strongly simplified chemical models in the analysis to most clearly expose the origin of the observed changes of D as a function of the nature of X and also of the configuration (trans/cis).

We focus here on points a, b, and d, since a systematic DFT calibration study for ZFSs that includes all technical aspects of the theory will be presented elsewhere.

Experimental Section

General Procedures. Reagents and solvents (analytical grade) were purchased from Aldrich and Fluka and used as received. Tris-2-picolylamine or tris(2-pyridylmethyl)amine (tpa) was prepared according to the literature method.[11] Infrared spectra were recorded on a Perkin-Elmer Spectrum GX FTIR spectrometer. Elemental analyses were performed by the Service Central d'Analyse du CNRS at Vernaison, France.

Synthesis of $[Mn(tpa)X_2]$ (X = I (1), Br (2), and Cl (3)). **Complex 1**. To a stirred solution of tpa (79.57 mg, 0.274 mmol) in 30 mL of methanol was added 1 equiv of MnI_2 (84.59 mg, 0.274 mmol). The resulting colorless solution was heated to reflux for 1 h under an argon atmosphere and then cooled to room temperature and filtered. Colorless single crystals were obtained by slow diffusion of ethyl acetate into the filtrate. Complexes **2** and **3** were prepared according to the same procedure using 80.6 mg of tpa and 59.2 mg of $MnBr_2$ and 80.4 mg of tpa and 34.8 mg of $MnCl_2$, respectively. Yield: 0.1453 g (88%). Elemental Anal. Calcd for **1** ($C_{18}H_{18}MnN_4I_2$ (599.14)): C, 36.08; H, 3.03; N, 9.35; I, 42.36. Found: C, 36.05; H, 3.16; N, 9.46; I, 42.09. IR (KBr, cm^{-1}): ν = 3445 (vs), 1601 (s), 1571 (m), 1478 (m), 1456 (w), 1441 (s), 1421 (m), 1394 (w), 1354 (m), 1316 (w), 1289 (m), 1273 (w), 1233 (w), 1154 (w), 1144 (w), 1117 (m), 1095 (m), 1048 (m), 1015 (s), 994 (w), 968 (w), 958 (w), 937 (w), 911 (m), 899 (w), 854 (w), 818 (w), 771 (s), 754 (s), 738 (w), 721 (w), 651 (w), 639 (m), 514 (w), 499 (w), 442 (w), 413 (m), 336 (w).

Complex 2. Yield: 0.1255 g (90%). Elemental Anal. Calcd for **2** ($C_{18}H_{18}MnN_4Br_2$ (505.12)): C, 42.80; H, 3.59; N, 11.09; Br, 31.64. Found: C, 42.73; H, 3.68; N, 11.19; Br, 31.88. IR (KBr, cm^{-1}): ν = 3445 (vs), 1602 (s), 1572 (m), 1479 (m), 1457 (w), 1443 (s), 1422 (m), 1396 (w), 1354 (m), 1317 (w), 1294 (m), 1272 (w), 1231 (w), 1157 (w), 1146 (w), 1120 (m), 1096 (m), 1048 (m), 1015 (s), 997 (w), 970 (w), 960 (w), 938 (w), 911 (w), 894 (w), 854 (w), 818 (w), 774 (s), 763 (s), 741 (w), 723 (w), 650 (w), 639 (m), 515 (w), 500 (w), 440 (w), 413 (m), 339 (w).

Complex 3. Yield: 0.1054 g (91%). Elemental Anal. Calcd for **3** ($C_{18}H_{18}MnN_4Cl_2$ (416.21)): C, 51.94; H, 4.36; N, 13.46; Cl, 17.03. Found: C, 51.76; H, 4.51; N, 13.59; Cl, 16.96. IR (KBr, cm^{-1}): ν = 3419 (vs), 1602 (s), 1571 (m), 1479 (m), 1458 (w), 1442 (s), 1422 (s), 1396 (w), 1354 (m), 1317 (w), 1295 (m), 1272 (w), 1231 (w), 1158 (w), 1146 (w), 1121 (m), 1096 (m), 1048 (m), 1015 (s), 997 (w), 970 (w), 961 (w), 939 (w), 911 (w), 895 (w), 854 (w), 819 (w), 774 (s), 764 (s), 741 (w), 723 (w), 650 (w), 639 (m), 515 (w), 499 (w), 440 (w), 412 (m), 340 (w).

Physical Measurements. IR spectra were obtained using a Perkin-Elmer Spectrum GX spectrophotometer, controlled by a Dell Optiplex GXa computer. Spectra were recorded on a solid sample at 1% by mass in a pellet of KBr. High-frequency and high-field EPR spectra were recorded on a laboratory-made spectrometer[12] using powder samples pressed in pellets to avoid preferential orientation of the crystallites in the strong magnetic field. Gunn

(5) (a) Boca, R. *Coord. Chem. Rev*. **2004**, *248*, 757. (b) Neese, F.; Solomon, E. I. In *Magnetoscience—From Molecules to Materials*; Miller, J. S., Drillon, M., Eds.; Wiley: New York, 2003; Vol. IV; p 345. (c) Neese, F. In *Calculation of NMR and EPR Parameters. Theory and Applications*; Kaupp, M., Bühl, M., Malkin, V., Eds.; Wiley-VCH: Weinheim, Germany, 2004; pp 541−564. (d) Neese, F. *Biological Magnetic Resonance*; Hanson, G., Berliner. J., Eds., in press.

(6) Neese, F.; Solomon, E. I. *Inorg. Chem*. **1998**, *37*, 6568.

(7) (a) Pederson, M. R.; Khanna, S. N. *Phys. Rev. B: Condens. Matter Mater. Phys*. **1999**, *60*, 9566. (b) Kortus, J. *Phys. Rev*. **2002**, *66*, 092403. (c) Ray, K.; Begum, A.; Weyhermüller, T.; Piligkos, S.; van Slageren, J.; Neese, F.; Wieghardt, K. *J. Am. Chem. Soc*. **2005**, *127*, 4403. (d) Schöneboom, J. Neese, F.; Thiel, W. *J. Am. Chem. Soc*. **2005**, *127*, 5840.

(8) (a) Reviakine, R.; Arbuznikov, A.; Tremblay, J.-C.; Remenyi, C.; Malkina, O. L.; Malkin, V. G.; Kaupp, M. *J. Chem. Phys*. **2006**, *125*, 054110. (b) Aquino, F.; Rodriguez, J. H. *J. Chem. Phys*. **2005**, *123*, 204902.

(9) Petrenko, T. T.; Petrenko, T. L.; Bratus, V. Y. *J. Phys.: Condens. Matter* **2002**, *14*, 12433.

(10) (a) Vahtras, O.; Loboda, O.; Minaev, B.; Agren, H.; Ruud, K. *Chem. Phys*. **2002**, *279*, 133. (b) Loboda, O.; Minaev, B.; Vahtras, O.; Schimmelpfennig, B.; Agren, H.; Ruud, K.; Jonsson, D. *Chem. Phys*. **2003**, *286*, 127. (c) Shoji, M.; Koizumi, K.; Hamamoto, T.; Taniguchi, T.; Takeda, R.; Kitagawa, Y.; Kawakami, T.; Okumura, M.; Yamanaka, S.; Yamaguchi, K. *Polyhedron* **2004**, *24*, 2708. (d) Sinnecker, S.; Neese, F. *J. Phys. Chem. A* **2006**, *110*, 12267−12275.

(11) Karlin, K. D.; Hayes, J. C.; Hutchinson, J. P.; Zubieta, J. *Inorg. Chem*. **1982**, *21*, 4106.

(12) (a) Barra, A.-L.; Brunel, L.-C.; Robert, J. B. *Chem. Phys. Lett*. **1990**, *165*, 107. (b) Muller, F.; Hopkins, M. A.; Coron, N.; Gryndberg, M.; Brunel, L.-C.; Martinez, G. *Rev. Sci. Instrum*. **1989**, *60*, 3681.

Table 1. Principal Crystallographic Data and Parameters for the [Mn(tpa)X_2] Complexes (X = I (**1**), Br (**2**), and Cl (**3**))

	compound		
	1	**2**	**3**
chemical formula	$C_{18}H_{18}I_2MnN_4$	$C_{18}H_{18}Br_2MnN_4$	$C_{18}H_{18}Cl_2MnN_4$
fw	599.10	505.12	416.2
cryst syst	monoclinic	monoclinic	monoclinic
space group	*P*2(1)/*n*	*P*2(1)/*n*	*P*2(1)/*n*
a/Å	9.1075(18)	9.0109(18)	9.0260(18)
b/Å	16.228(3)	15.951(3)	15.876(3)
c/Å	14.137(3)	13.459(3)	13.278(3)
α/deg	90	90	90
β/deg	91.86(3)	96.33(3)	98.84(3)
γ/deg	90	90	90
volume/Å^3	2088.2(7)	1922.8(7)	1880.1(7)
T/K	298(2)	193(2)	298(2)
λ/Å	0.71073	0.71073	0.71073
density/mg m^{-3}	1.906	1.745	1.470
Z	4	4	4
μ/mm^{-1}	3.597	4.851	0.994
F(000)	1140	996	852
reflns collected	13004	7395	7276
R1[a]	0.0298	0.0352	0.0386
wR2[b]	0.0511	0.0844	0.0772

[a] $R1 = \sum||F_o| - |F_c||/\sum|F_o|$. [b] $wR2 = [(\sum w(|F_o| - |F_c|)^2/\sum wF_o^2)]^{1/2}$.

diodes operating at 95 and 115 GHz and equipped with a second- and third-harmonic generator were used as the radiation source. The magnetic field was produced by a superconducting magnet (0−12 T).

Crystal Structure Determination. Diffraction data were collected on a Bruker SMART diffractometer with Mo Kα radiation. The crystals of the complexes were of dimensions 0.2 × 0.2 × 0.2 mm for **1**, 0.3 × 0.3 × 0.2 mm for **2**, and 0.4 × 0.4 × 0.2 mm for **3**. The crystallographic data are summarized in Tables 1 and 2. All calculations were effected using the *SHELXTL* computer program.[13] The CCDC reference numbers are 610221 (**1**), 610223 (**2**), and 610224 (**3**).

Theoretical Calculations. All calculations reported in this work were performed with the *ORCA* program package.[14] The structure of the models *cis, trans*-[$Mn^{II}(NH_3)_4(X)_2$] (X = F, Cl, Br, I) were fully optimized using the BP86 functional[15] and the TZVP basis set.[16] As discussed in more detail below, scalar relativistic effects were taken into account for the Br and I derivatives using our implementation of van Wüllen's model potential approximation[17] to the ZORA equations.[18] In the geometry optimizations with the ZORA model we have used the one-center approximation since it has been shown to lead to negligible errors in the computed structures.[19]

EPR properties were calculated using spin-unrestricted DFT together with both the spin−orbit meanfield (SOMF)[20] representation of the SOC operator in the implementation[21] as well as the effective nuclear charge SOC-Hamiltonian parametrized by Koseki et al.[22] In the latter, the SOC is represented by a sum over atomic contributions

$$\hat{H}_{SOC} = \frac{\alpha^2}{2}\sum_i\sum_A \frac{Z_A^{eff}}{|\mathbf{r}_i - \mathbf{R}_A|^3}\hat{\mathbf{l}}_{iA}\hat{\mathbf{s}}_i \quad (2)$$

where α is the fine-structure constant (∼$^1/_{137}$ in atomic units), with *i* sums over electrons and *A* sums over atoms; $\mathbf{r}_i$ is the position of the *i*th electron, and $\mathbf{R}_A$ is the position of nucleus *A*. The operators $\hat{\mathbf{s}}_i$ and $\hat{\mathbf{l}}_{iA}$ represent the spin of the *i*th electron and its angular momentum relative to atom *A*, respectively. Z_A^{eff} is a semiempirically chosen effective nuclear charge that is generally smaller than the true nuclear charge Z_A to compensate for the neglect of two-electron terms that essentially provide a screening. This representation is partially used below despite its somewhat inferior accuracy since it provides the opportunity to separate many-center contributions to the SOC as well as to "quench" the contributions of individual atoms to the SOC to obtain insight into the nature of the calculated effects. For the calculation of the spin−spin contribution to the ZFS, we refer to ref 4, whereas the SOC contribution was calculated with the method of Pederson and Khanna[7a] to allow for easier comparison with the work of other authors that have implemented the same methodology. Specifically, the SS and SOC contributions to the ***D*** tensor are calculated as

$$D_{kl}^{(SS)} = \frac{g_e^2}{4}\frac{\alpha^2}{S(2S-1)}\sum_{\mu\nu}\sum_{\kappa\tau}\{P_{\mu\nu}^{\alpha-\beta}P_{\kappa\tau}^{\alpha-\beta} - P_{\mu\kappa}^{\alpha-\beta}P_{\nu\tau}^{\alpha-\beta}\}\langle\mu\nu|r_{12}^{-5}\{3r_{12,k}r_{12,l} - \delta_{kl}r_{12}^2\}|\kappa\tau\rangle \quad (3)$$

$$\begin{aligned} D_{KL}^{(SOC)} = &-\frac{1}{4S^2}\sum_{i_\beta,a_\beta}\frac{\langle\psi_i^\beta|h_K^{SOC}|\psi_a^\beta\rangle\langle\psi_a^\beta|h_L^{SOC}|\psi_i^\beta\rangle}{\epsilon_a^\beta - \epsilon_i^\beta} \\ &-\frac{1}{4S^2}\sum_{i_\alpha,a_\alpha}\frac{\langle\psi_i^\alpha|h_K^{SOC}|\psi_a^\alpha\rangle\langle\psi_a^\alpha|h_L^{SOC}|\psi_i^\alpha\rangle}{\epsilon_a^\alpha - \epsilon_i^\alpha} \\ &+\frac{1}{4S^2}\sum_{i_\alpha,a_\beta}\frac{\langle\psi_i^\alpha|h_K^{SOC}|\psi_a^\beta\rangle\langle\psi_a^\beta|h_L^{SOC}|\psi_i^\alpha\rangle}{\epsilon_a^\beta - \epsilon_i^\alpha} \\ &+\frac{1}{4S^2}\sum_{i_\beta,a_\alpha}\frac{\langle\psi_i^\alpha|h_K^{SOC}|\psi_a^\alpha\rangle\langle\psi_a^\alpha|h_L^{SOC}|\psi_i^\alpha\rangle}{\epsilon_a^\alpha - \epsilon_i^\beta} \quad (4) \end{aligned}$$

Here, *S* is the total spin of the electronic ground state (=$^5/_2$ here), g_e (=2.002319...) is the free electron *g* value, α (∼$^1/_{137}$) is the fine structure constant, $P^{\alpha-\beta}$ is the spin-density matrix in the atomic orbital basis $\{\varphi_\mu\}$, which is used to expand the molecular spin-orbitals as $\psi_p^\sigma = \sum_\mu c_{\mu p}^\sigma\varphi_\mu$ with orbital energies ϵ_p^σ ($p = i$ and *a* refers to occupied and unoccupied spin-orbitals, respectively). The operator $r_{12}^{-5}\{3r_{12,k}r_{12,l} - \delta_{kl}r_{12}^2\}$ represents the dipolar spin−spin coupling between a pair of electrons, and h_K^{SOC} is the *K*th spatial component of a reduced SOC operator (*K*,*L* = *x*, *y*, *z*).[6,21]

Results and Analysis

To obtain structural data on a series of dihalide Mn^{II} complexes with a cis configuration, we have used the

(13) Sheldrick, G. M. *SHELXTL-Plus, Structure Determination Software Programs*, version 5.1; Bruker-AXS Inc.: Madison, WI, 1998.
(14) Neese, F. *ORCA—An ab Initio, Density Functional and Semiempirical Program Package*, version 2.4.55; Universität Bonn: Bonn, Germany. The program can be downloaded free of charge from http://www.thch.uni-bonn.de/tc/orca.
(15) (a) Becke, A. D. *Phys. Rev. A* **1988**, *38*, 3098. (b) Perdew, J. P. *Phys. Rev. B: Condens. Matter Mater. Phys.* **1986**, *33*, 8822.
(16) Schäfer, A.; Huber, C.; Ahlrichs, R. *J. Chem. Phys*. **1994**, *100*, 5829.
(17) van Wüllen, C. *J. Chem. Phys.* **1998**, *109*, 392.
(18) van Lenthe, E.; Sniijders, J. G.; Baerends, E. J. *J. Chem. Phys*. **1996**, *105*, 6505.
(19) van Lenthe, J. H.; Faas, S.; Sniijders, J. G. *Chem. Phys. Lett*. **2000**, *328*, 107.
(20) Hess, B. A.; Marian, C. M.; Wahlgren, U.; Gropen, O. *Chem. Phys. Lett*. **1996**, *251*, 365.
(21) Neese, F. *J. Chem. Phys.* **2005**, *122*, 034107.
(22) (a) Koseki, S.; Gordon, M. S.; Schmidt, M. W.; Matsunaga, N. *J. Phys. Chem.* **1995**, *99*, 12764. (b) Koseki, S.; Schmidt, M. W.; Gordon, M. S. *J. Phys. Chem. A* **1998**, *102*, 10430.

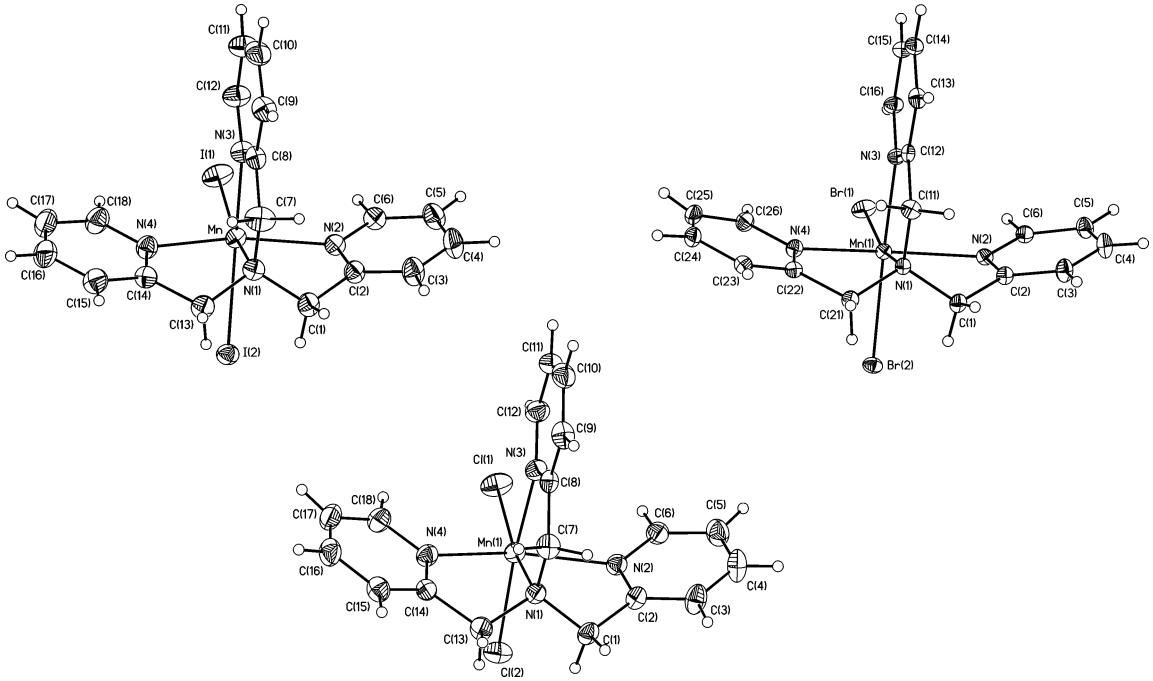

Figure 1. *ORTEP* diagrams showing the molecular structures of complexes **1**−**3**.

Table 2. Selected Bond Distances (Å) and Angles (deg) for the $[Mn(tpa)X_2]$ Complexes (X = I (**1**), Br (**2**), and Cl (**3**))

	compound		
	1	**2**	**3**
Mn−X(1)	2.8011(9)	2.5771(10)	2.4219(11)
Mn−X(2)	2.8773(7)	2.6187(7)	2.4542(8)
Mn−N(1)	2.363(2)	2.372(3)	2.396(2)
Mn−N(2)	2.267(2)	2.275(3)	2.2943(19)
Mn−N(3)	2.318(3)	2.327(2)	2.3525(19)
Mn−N(4)	2.263(3)	2.266(3)	2.285(2)
N(1)−Mn−N(2)	73.32(9)	73.07(9)	72.54(7)
N(1)−Mn−N(3)	74.56(9)	74.01(9)	72.87(7)
N(1)−Mn−N(4)	73.15(9)	72.61(9)	72.00(7)
N(2)−Mn−N(3)	86.53(9)	83.50(9)	81.23(7)
N(3)−Mn−N(4)	84.06(10)	83.84(9)	83.45(7)
N(2)−Mn−N(4)	146.47(9)	145.49(10)	144.13(7)
N(1)−Mn−X(1)	167.59(6)	166.26(6)	164.08(5)
N(1)−Mn−X(2)	96.10(6)	95.01(6)	94.00(5)
N(2)−Mn−X(1)	105.57(6)	106.65(7)	106.98(6)
N(2)−Mn−X(2)	92.33(7)	93.66(6)	94.50(5)
N(3)−Mn−X(1)	93.06(6)	92.27(7)	91.27(5)
N(3)−Mn−X(2)	170.53(6)	169.02(7)	166.85(5)
N(4)−Mn−X(1)	107.02(7)	105.81(7)	105.60(6)
N(4)−Mn−X(2)	91.80(7)	92.74(7)	93.14(6)
X(1)−Mn−X(2)	96.297(18)	98.71(2)	101.87(3)

tetradentate tpa ligand to impose this configuration. The electronic properties of these complexes were investigated by HF-EPR on powder samples at high frequencies (95−285 GHz). The spin Hamiltonian parameters of these complexes have also been calculated theoretically by DFT.

Synthesis and Crystal Structure Determination. The $[Mn(tpa)X_2]$ (X = I (**1**), Br (**2**), and Cl (**3**)) complexes have been isolated from a mixture of an equimolar amount of anhydrous MnX_2 and tpa in methanol. Single crystals were obtained by slow diffusion of ethyl acetate into these methanolic solutions, and their crystal structures have been determined by X-ray diffraction. Tables 1 and 2 provide the principal crystallographic data together with selected bond distances and angles, and Figure 1 displays their *ORTEP* views.

The Mn^{II} ions in complexes **1**−**3** are pseudo-octahedrally coordinated by four nitrogen atoms from tpa and two halide atoms. The halide ligands are cis in all cases, with this configuration being imposed by the nature of the tpa ligand. The $Mn-N_{tpa}$ (Mn−N(1) and Mn−N(3)) bonds trans to the X atoms (2.318−2.396 Å) are consistently longer than the other $Mn-N_{tpa}$ bonds Mn−N(2) and Mn−N(4) (2.263−2.294 Å). This trans effect has already been observed in $[Mn_2^{II}(\mu\text{-}O_2CCH_3)_2(tpa)_2]$,[23] $[Mn^{II}(tpa)(TCNQ)(CH_3OH)]^{3+}$ (TCNQ = tetracyanoquinodimethane), and $[Mn_2^{II}(CA)(tpa)_2]^{2+}$ [24] (CA = chloranilic acid).

The Mn−X bond lengths for **2** and **3** are located in the range of values found in other Mn^{II}−X complexes (Mn−Br, 2.490−2.666 Å;[3f,25] Mn−Cl, 2.224−2.538 Å[3f,3h,25a,25e,26]) whereas the Mn−I bond lengths of 2.8773(7) and 2.8011(9) Å for **1** are slightly longer than those expected for such complexes (Mn−I, 2.661−2.767 Å[3f,25,27]). The decrease of the bond distances in the order Mn−I > Mn−Br > Mn−Cl

(23) Oshio, H.; Ino, E.; Mogi, I.; Ito, I. *Inorg. Chem.* **1993**, *32*, 5697.
(24) Xiang, D. F.; Duan, C. Y.; Tan, X. S.; Liu, Y. J.; Tang, W. X. *Polyhedron* **1998**, *17*, 2647.
(25) (a) Turner, P.; Gunter, M. J.; Skelton, B. W.; White, A. H. *Aust. J. Chem.* **1998**, *51*, 853. (b) Delaunay, J.; Hugel, P. *Inorg. Chem.* **1986**, *25*, 3957. (c) Butcher, R. J.; Sinn, E. *J. Chem. Soc., Dalton Trans.* **1976**, 1186. (d) Girolami, G. S.; Wilkinson, G. *J. Am. Chem. Soc.* **1983**, *105*, 6752. (e) Tajiri, Y.; Ichihashi, M.; Mibuchi, T.; Wakita, H. *Bull. Chem. Soc. Jpn.* **1986**, *59*, 1155.
(26) (a) Shuangxi, W.; Ying, Z.; Fangjie, Z.; Qiuying, W.; Liufang, W. *Polyhedron* **1992**, *11*, 1909. (b) Di Vaira, M.; Mani, F. *J. Chem. Soc., Dalton Trans*. **1990**, 191. (c) Ferrari, M. B.; Fava, G. G.; Pelizzi, P.; Tarasconi, P.; Tosi, G. *J. Chem. Soc., Dalton Trans*. **1987**, 227. (d) Phillips, F. L.; Shreeve, F. M.; Skapski, A. C. *Acta Crystallogr*. **1976**, *B32*, 687. (e) Oki, R.; Bommarreddy, P. R.; Zhang, H.; Hosmane, N. *Inorg. Chim. Acta* **1995**, *231*, 109. (f) Lah, M. S.; Chun, H. *Inorg. Chem.* **1997**, *36*, 1782. (g) Goodson, P. A.; Oki, A. R.; Hodgson, D. J. *Inorg. Chim. Acta* **1990**, *177*, 59. (h) McCann, S.; McCann, M.; Casey, R. M. T.; Jackman, M.; Devereux, M.; McKee, V.; *Inorg. Chim. Acta* **1998**, *279*, 24.

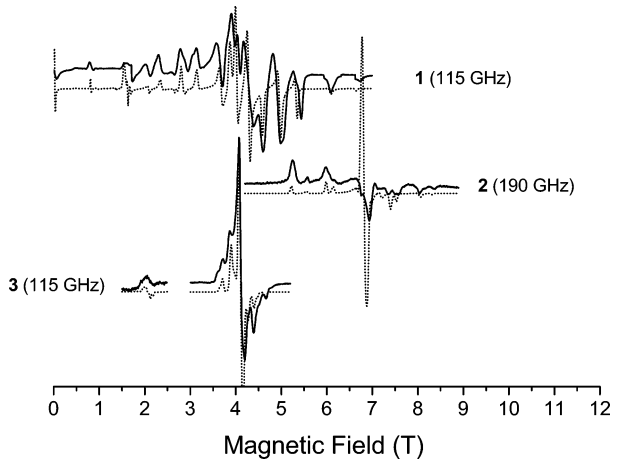

Figure 2. Experimental (solid line) and simulated (dotted line) neat powder HF-EPR spectra of complexes **1** (115 GHz), **2** (190 GHz), and **3** (115 GHz) recorded at 30 K. Parameters used for the simulation: **1**, $D = -0.600(5)$ cm^{-1}, $E = 0.095(5)$ cm^{-1}, $g_x = 1.99(1)$, $g_y = 1.98(1)$, $g_z = 2.00(1)$. **2**, $D = -0.360(4)$ cm^{-1}, $E = 0.073(2)$ cm^{-1}, $g_x = 2.00(1)$, $g_y = 1.98(1)$, $g_z = 2.00(1)$. **3**, $D = +0.115(2)$ cm^{-1}, $E = 0.020(1)$ cm^{-1}, $g_x = 1.97(1)$, $g_y = 2.00(1)$, $g_z = 2.00(1)$.

is correlated to the electronegativity properties of the anions (I < Br < Cl). The angles around the Mn ions observed in **1**−**3** are characteristic of Mn^{II} complexes containing the tpa ligand due to its tetradentate spatially constrained nature.[23,24]

Multifrequency EPR Experiments. Powder HF-EPR spectra have been recorded for each complex at frequencies between 95 and 285 GHz over the temperature range of 5−60 K. Figure 2 displays 30 K EPR spectra of the complexes recorded at different frequencies. At temperatures lower than 30 K, the shape of the spectra indicates saturating conditions. This problem is recurrent for mononuclear Mn^{II} complexes with slow electronic relaxation rates.[3h] Unfortunately, the ^{55}Mn-hyperfine structure was not resolved in these experiments, which is presumably due to intermolecular dipole−dipole interactions. The analysis of the HF-EPR spectra of **1**−**3** has been performed as described previously[3f−h] and will therefore not be further elaborated.

Under high-field limit conditions ($D \ll h\nu$), the ZFS parameters govern the shape of the Mn^{II} EPR spectra. Accordingly, they have similar shapes at all frequencies and the resonances are simply shifted as $B' = B\nu'/\nu$, where B and B' are the field locations of the same line at ν and ν', respectively. In the spectra shown in Figure 2, $\Delta M_s > 1$ transitions located below 2.5 T are only observable for complexes **1** and **3** since the spectra have been recorded at lower frequencies compared with those of **2**. All of the other detected features correspond to $\Delta M_s = 1$ transitions associated with the three principal magnetic axes *x*, *y*, and *z*. The spectrum of **1** has the largest total width (around 5.2 T) compared with **2** and **3** (3.0 and 1.2 T, respectively). This is directly correlated with the magnitude of *D*, which decreases from **1** to **3**. A larger number of transitions is resolved in the EPR spectra of **1** and **2** (Figure 2) compared with those of **3**, since the larger the value of *D*, the better the transitions are separated in the field. The number of detectable transitions also depends on the *E*/*D* ratio. With *E*/*D* equal or close to 0 or $^1/_3$, only 5 transitions are expected, whereas for intermediate *E*/*D* ratios, up to 13 transitions are expected (in the isotropic case where $g_x = g_y = g_z$). The accurate determination of the spin Hamiltonian parameters from simulations of the experimental EPR spectra using a full-matrix diagonalization procedure of the SH eq 5 corroborates this reasoning.

$$H = \beta \mathbf{B} \mathbf{g} S + D[S_z^2 - {}^1/_3 S(S+1)] + E(S_x^2 - S_y^2) \quad (5)$$

For each complex, the EPR spectra were reproduced at all frequencies and temperatures, with the unique set of parameters given in Figure 2 and also reported in Table 3. Comparisons of simulated and experimental spectra are presented in Figure 2. The sign of *D* has been unambiguously established on the basis of the low-temperature HF-EPR spectra.

Table 3 also reports SH parameters determined for other mononuclear dihalide Mn^{II} complexes described in the literature. The *D* values obtained for **1**−**3** are very close to those of the phen series, confirming the important effect of the configuration of the two halides on the magnitude of *D* in six-coordinate complexes. A cis versus trans arrangement of the anions decreases the *D* values by almost a factor of 2. The general trend of the *D* values as a function of the nature of the halide is also still observed within the tpa series. The sign of *D* has been determined only in few cases since HF-EPR experiments at low temperature are required for this purpose.

Table 3. Electronic Parameters and Coordination Number for Mn^{II} Dihalide Complexes Described in the Literature and in This Work[a]

complexes[b]	coord no.	D (cm^{-1})	E (cm^{-1})	$\lvert E/D \rvert$	ref
cis-**[**Mn**(**tpa**)**I$_2$]	6	−0.600	0.095	0.158	this work
cis-[Mn(phen)$_2$I$_2$]	6	0.590	0.145	0.246	3c
trans-[Mn(pic)$_4$I$_2$]	6	0.999	≤0.005	≤0.005	3c
trans-[Co(Mn)(pyr)$_4$I$_2$]	6	0.932	0.0196	0.021	3b
[Mn(terpy)I$_2$]	5	+1.000	0.19	0.19	3f
[Mn(OPPh$_3$)$_2$I$_2$]	4	0.906	0.223	0.246	3d
[Zn(Mn)(N$_2$H$_4$)$_2$I$_2$]	4	1.21	0.023	0.019	3a
cis-**[**Mn**(**tpa**)**Br$_2$**]**	6	−0.360	0.073	0.203	this work
cis-[Mn(phen)2Br$_2$]	6	0.359	0.074	0.21	3c
trans-[Mn(pic)$_4$Br$_2$]	6	0.626	≤ 0.003	≤ 0.005	3c
trans-[Co(Mn)(pyr)$_4$-Br$_2$]	6	0.590	0.0032	0.0054	3b
trans-[Mn(X-pyr)$_4$Br$_2$]	6	0.650	0.0065	0.01	3e
[Mn(terpy)Br$_2$]	5	+0.605	0.159	0.26	3f
[Mn(OPPh$_3$)$_2$Br$_2$]	4	0.507	0.134	0.263	3d
[Zn(Mn)(N2H$_4$)$_2$Br$_2$]	4	0.71	0	0	3a
cis-[Mn(tpa)Cl$_2$]	6	+0.115	0.020	0.174	this work
cis-[Mn(phen)2Cl$_2$]	6	0.124	0.005	0.04	3c
trans-[Mn(pic)$_4$Cl$_2$]	6	0.186	0	0	3c
trans-[Co(Mn)Mn-(pyr)$_4$Cl$_2$]	6	0.208	0	0	3b
trans-[Mn(X-pyr)$_4$Cl$_2$]	6	0.188	0.011	0.06	3e
[Mn(terpy)Cl$_2$]	5	−0.260	0.075	0.29	3f
[Mn(OPPh$_3$)$_2$Cl$_2$]	4	0.165	0.045	0.273	3d
[Zn(Mn)(N$_2$H$_4$)$_2$Cl$_2$]	4	0.29	0.0044	0.0015	3a

[a]The sign of *D* is specified when it has been determined. [a] Abbreviations: phen = *o*-phenanthroline; pic = γ-picoline; pyr = pyridine; terpy = 2,2′:6′,2″-terpyridine; OPPh$_3$ = triphenylphosphine oxide; X-pyr = O^{i}Pr$_2$SiOCH$_2$-pyr.

(27) (a) Aviles, T.; de C. T. Larrondo, M. A. A. F.; Piedade, M. F. M.; Teixeira, G. *J. Organomet. Chem.* **1990**, *388*, 143. (b) Hebendanz, N.; Köhler, F. H.; Müller, G. *Inorg. Chem.* **1984**, *23*, 3044.

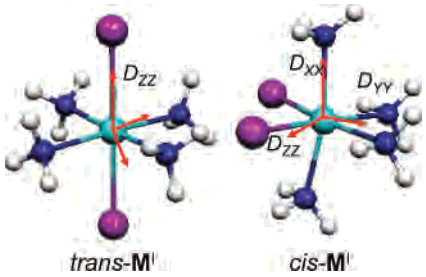

Figure 3. Representation of the M^I models. The orientations of the ***D*** tensor are also shown.

Table 4. Experimental and Calculated Electronic Parameters for Complexes **1**−**3**

complexes	D_{exp} (cm^{-1})	D_{calc} (cm^{-1})	D_{SS} (cm^{-1})	D_{SOC} (cm^{-1})	E/D_{exp}	E/D_{calc}
1	−0.600	−0.868	−0.009	−0.859	0.16	0.16
2	−0.360	−0.510	−0.010	−0.500	0.19	0.24
3	+0.115	+0.155	+0.005	+0.150	0.20	0.17

From Table 3, it appears that the *E*/*D* ratio depends predominantly on the nature of the neutral ligand. With monodentate ligands such as pyr, the systems are quasi-axial (*E*/*D* = 0), whereas with bi-, tri-, or tetradentate ligands, the steric constraints cause an increase in the *E*/*D* ratio for six-coordinate complexes. The *E*/*D* ratios for **1**−**3** lie between 0.15 and 0.23, reflecting the distortions observed in their X-ray structures.

Density Functional Calculations. A. Calculations on Complexes 1−3. To understand the trends in the observed *D* and *E*/*D* values, a systematic DFT study has been carried out. The calculations on the actual systems studied experimentally above were initiated from the crystal structures. The EPR parameters predicted at the optimized geometries (BP86/TZVP) are collected in Table 4 and show reasonable agreement between the experimental and the calculated ZFS parameters. The absolute value of *D* is consistently overestimated, but the sign and the trend over the chemical series are predicted accurately. Consequently, the calculations can be used to qualitatively understand the origin of the observed effects. However, since the focus of the investigation is on the qualitative interpretation on a related series of compounds rather than on their individual members, the simplest reasonable chemical models have been chosen for a detailed study, namely, $[Mn(NH_3)_4(X)_2]$ (X = F, Cl, Br, I). It will be shown below that the calculations yield important clues to the origin of the observed variations in the ZFS parameters. A detailed methodology-oriented study on a much more extensive series of Mn^{II} complexes will be reported elsewhere to establish the typical error bars of the employed methodology.

B. Model Study. Detailed calculations were carried out for *trans*- and *cis*-$[Mn^{II}(NH_3)_4(X)_2]$ (X = I, Br, Cl and F; $S = {}^5/_2$) models, leading to a total of eight structures (labeled *cis*, *trans*-$\mathbf{M}^X$, with X = F, Cl, Br, I). Attention was given to: (a) variation of *D* with the nature of the halide; (b) variation of *D* with the arrangement of the halides; and (c) individual SOC and SS coupling contributions to *D*.

B.1. Geometric Structure. Geometry optimizations at the BP86/TZVP level were performed for all eight models starting from pseudo-octahedral coordination geometries. The optimized structures of *trans*-$\mathbf{M}^I$ *and cis*-$\mathbf{M}^I$ are shown in Figure 3, and detailed metrical parameters obtained for the eight models are collected in Table 5. Scalar relativistic effects at the ZORA(MP) level have been included for the $\mathbf{M}^I$, $\mathbf{M}^{Br}$, and $\mathbf{M}^{Cl}$ derivatives. For $\mathbf{M}^I$, the changes in the Mn−N/X distances due to relativity are less than 5%, and for M^{Br}, the changes amount to less than 4%, whereas for $\mathbf{M}^{Cl}$, they are less than 1%. Consequently, the ZORA method has only been employed for the calculations on the $\mathbf{M}^I$ and $\mathbf{M}^{Br}$ models. For $\mathbf{M}^F$ and *cis*-$\mathbf{M}^{Cl}$ models, the optimized structures were highly distorted from idealized octahedral geometries. Since they cannot be related to real molecules, they were dropped from further analysis.

Where comparison is meaningful, the optimized structures are in excellent agreement with experimental metrical data. The Mn−N bond distances vary from 2.26 to 2.36 Å whereas the Mn−X distance increases significantly with increasing size and decreasing electronegativity of the halide, as expected (2.8 Å <Mn−I < 2.9 Å; 2.6 Å <Mn−Br < 2.7 Å; and 2.52 Å <Mn−Cl < 2.53 Å). The Mn−X distances in $\mathbf{M}^I$, $\mathbf{M}^{Br}$, and $\mathbf{M}^{Cl}$ are, nevertheless, slightly longer (by ∼5 pm) than those found in the crystallographically characterized Mn^{II} complexes (see Table 2), which is typical of the BP86 functional used in this study.[28]

In the trans models, the octahedral angles are almost perfectly retained for $\mathbf{M}^I$ and $\mathbf{M}^{Br}$ whereas for $\mathbf{M}^{Cl}$, they differ from the expected values (90 and 180°). As an example, the X−Mn−X angle is equal to 160° in *trans*-$\mathbf{M}^{Cl}$. Regarding the cis series, the optimization of $\mathbf{M}^I$ and $\mathbf{M}^{Br}$ had to be performed using geometrical constraints to prevent one halide from being ejected from the coordination sphere during the optimization. The structures are characterized by a distorted octahedral geometry, as can be seen from the metrical parameters as well as the valency angles (N−Mn−N, 166° and 161° for the I and Br models, respectively; 169° < X−Mn−N < 173° for all models). The X−Mn−X angles were found to be 108° and 114° for $\mathbf{M}^I$ and $\mathbf{M}^{Br}$, respectively. These angles are comparable in all structures, showing that even if repulsion occurs between the two halide ligands, the increasing size of the halide is largely compensated by the longer Mn−X bond lengths. A similar trend has been observed experimentally in the tpa series, for which the X−Mn−X angle varies between 96° and 102° (Table 2).

B.2. Electronic Structure. Since ZFS parameters are frequently related to ligand-field models, an attempt was made to obtain some insight into the nature of the ligand field seen by the central Mn^{II} ion from the DFT calculations. It is, however, not evident what the best procedure for the connection is. The spin-unrestricted calculations lead to separate spin-up and spin-down orbitals. The former set of metal 3d-based orbitals is occupied and optimized in the variational process while the set of spin-down orbitals is unoccupied and unoptimized. As discussed, for example, in

(28) See, for example, the statements and references made in Neese, F. *J. Biol. Inorg. Chem.* **2006**, *11*, 702.

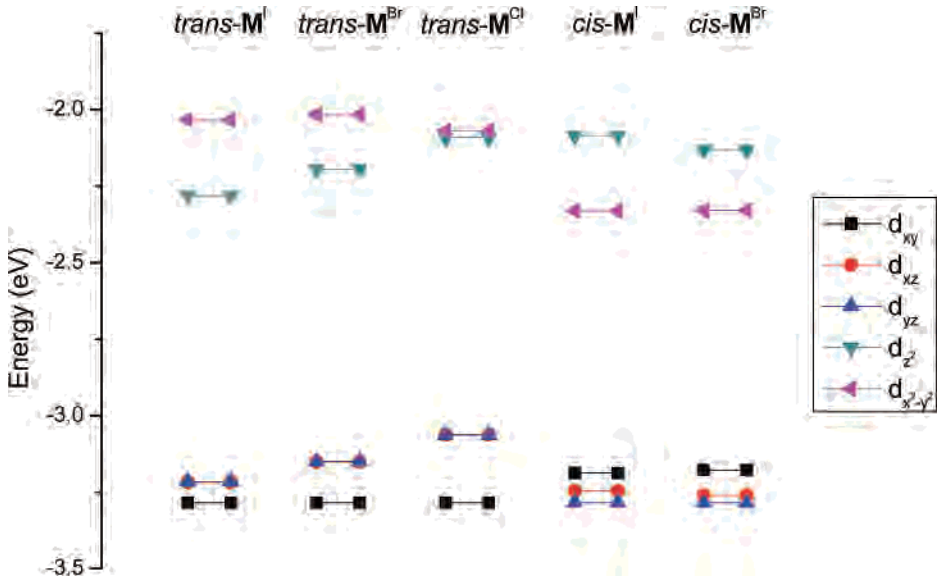

Figure 4. Energy diagrams obtained from the calculated energy (eV) of the quasi-restricted SOMOs for the M^X models.

Table 5. Calculated Metrical Parameters (in Å) Obtained from the Optimized Geometry of the $\mathbf{M}^X$ (X = I, Br, Cl, and F) Models

	trans-$\mathbf{M}^I$	*trans*-$\mathbf{M}^{Br}$	*trans*-$\mathbf{M}^{Cl}$	*trans*-$\mathbf{M}^F$	*cis*-$\mathbf{M}^I$	*cis*-$\mathbf{M}^{Br}$	*cis*-$\mathbf{M}^{Cl}$	*cis*-$\mathbf{M}^F$
Mn−N	2.311	2.305	2.321	2.313	2.353	2.352	2.338	2.35
Mn−N	2.311	2.304	2.311	2.303	2.349	2.349	2.336	2.344
Mn−N	2.309	2.297	2.310	2.297	2.286	2.289	2.266	2.241
Mn−N	2.303	2.294	2.300	2.293	2.285	2.289	2.265	2.34
Mn−X	2.844	2.691	2.528	2.097	2.900[a]	2.700[a]	2.653	2.090
Mn−X	2.841	2.652	2.523	2.063	2.800[a]	2.600[a]	2.487	2.047

[a] These bond lengths have been constrained to prevent ligand dissociation.

detail by Noodleman and co-workers,[29] the exchange stabilization of the occupied spin-up orbitals is so large that they fall energetically in the region of the ligand orbitals and mix so strongly with them that an analysis in terms of dominant Mn-d contributions is impossible. However, the metal character is still contained in the occupied space. Since the occupied space is invariant to unitary transformations, it is possible to find a display that reveals these orbitals, their shapes, and to some extent, also their energies in the clearest possible way. The set of orbitals that we prefer for such an analysis is the set of quasi-restricted molecular orbitals (QRMOs) introduced recently.[4,30] The five SOMOs of the QRMO solution correspond to the metal d-based MOs and can be employed for a ligand-field type analysis.

The resulting partial molecular orbital (MO) schemes are displayed in Figure 4. As expected, the results reveal that in the trans series, the tetragonal axis of the octahedron is along the X−Mn−X axis, whereas for the cis models, it is located along the N−Mn−N axis. Consequently, from an electronic point of view, the equatorial plane is formed by the four nitrogen atoms in the trans models and by the two halide and two nitrogen atoms in the cis structures. Since the halides are π donors in contrast to the amines, the tetragonal apparent distortion corresponds to an elongation in the trans models and to a compression in the cis ones. This is nicely reflected in the MO diagrams (Figure 4). For the trans models, the $d_{x^2-y^2}$ and d_{xz} and d_{yz} based MOs are the highest energy orbitals within the e_g and t_{2g} orbital sets, respectively (octahedral symmetry labels are kept for clarity). By contrast, the cis arrangement leads to d_{z^2} and d_{xy} being the most destabilized d-based MOs in the e_g and t_{2g} sets.

As expected, the effective electronic symmetry is higher in trans models (axial, pseudo C_{4v}) than in the cis models (rhombic). In pseudo C_{4v} symmetry, the d_{xz} and d_{yz} orbitals are degenerate under effective C_{4v} symmetry, whereas they are split in the cis models. The splitting reflects the differences in π interactions with the halide ligands.

In Table 6, the fractional population for each singly occupied molecular orbital (SOMO) in terms of the percentage contribution of the manganese, halide, and other atoms is provided. It becomes evident that there is a fairly large increase in the σ covalency from $\mathbf{M}^{Cl}$ to $\mathbf{M}^{Br}$ to $\mathbf{M}^I$ in all models. And this increase in the σ-bond strength is reflected in the orbital splitting of the e_g orbitals in Figure 4. By contrast, the variation in the π covalency is much less pronounced. Thus, the reverse trend in the orbital splitting in the π set of the trans models may best be explained with the electrostatic interaction of the metal ion with the halide, which becomes stronger as the halide becomes smaller and the metal−ligand distance becomes shorter. It is also evident that in the trans models, the d_{xy} orbital is at nearly constant energy, since it is not involved in any interaction with the halide ligand. This is different in the cis models, where the

(29) Noodleman, L.; Case, D. A. In *Inorganic Electronic Structure and Spectroscopy*; Solomon, E. I., Lever, A. B. P., Eds.; John Wiley & Sons: New York, 1999; Vol. 1, pp 661ff.
(30) Sinnecker, S.; Neese, F.; Noodleman, L.; Lubitz, W. *J. Am. Chem. Soc.* **2004**, *126*, 2613.

Table 6. Composition (%) of the SOMOs of the $\mathbf{M}^{X}$ Models from a Löwdin Analysis of the QRMOs[a]

	trans-$\mathbf{M}^{I}$			*trans*-$\mathbf{M}^{Br}$			*trans*-$\mathbf{M}^{Cl}$			*cis*-$\mathbf{M}^{I}$			*cis*-$\mathbf{M}^{Br}$		
	Mn	I	rest	Mn	Br	rest	Mn	Cl	rest	Mn	I	rest	Mn	Br	rest
d_{xy}	98.4	0	1.1	98.5	0	1.1	98.4	0	1.0	96.1	2.7	0.8	96.0	2.3	0.9
d_{xz}	96.6	2.7	0.4	97.1	2.3	0.2	96.8	2.1	0.7	98.1	0.3	1.1	97.1	0.2	2.5
d_{yz}	96.6	2.7	0.4	97.1	2.2	0.2	96.8	2.1	0.7	97.5	1.4	0.6	97.2	1.5	0.9
d_{z^2}	84.2	10.4	5.2	86.3	9.1	4.1	88.7	2.8	8.1	86.8	3.7	9.1	87.3	3.2	9.0
$d_{x^2-y^2}$	89.0	0	11.0	89.0	0	10.9	87.8	5.5	6.2	86.6	7.3	5.6	87.3	5.5	6.1

[a] rest corresponds to the addition of the contributions of the other atoms.

Table 7. Calculated EPR Parameters (Zero-Field Splitting Parameters, Isotropic *g* Value, and Isotropic Hyperfine Constant) for the $\mathbf{M}^{X}$ Models

	trans-$\mathbf{M}^{I}$	*trans*-$\mathbf{M}^{Br}$	*trans*-$\mathbf{M}^{Cl}$	*cis*-$\mathbf{M}^{I}$	*cis*-$\mathbf{M}^{Br}$
D (cm^{-1})	+1.358	+0.541	+0.212	+0.590	+0.355
D_{SOC} (cm^{-1})[a]	+1.301	+0.534	+0.177	+0.567	+0.334
$\alpha \rightarrow \alpha$[b]	+4.475	+0.544	+0.045	+1.730	+0.340
$\beta \rightarrow \beta$[b]	+5.460	+0.786	+0.086	+2.537	+0.536
$\alpha \rightarrow \beta$[b]	−4.857	−0.365	+0.069	−2.444	−0.325
$\beta \rightarrow \alpha$[b]	−3.777	−0.431	−0.023	−1.256	−0.217
D_{SS} (cm^{-1})[c]	+0.058	+0.008	+0.034	+0.023	+0.021
one center[d]	+0.033	+0.049	+0.017	+0.035	+0.020
two center[d]	+0.037	-0.033	+0.028	-0.008	+0.003
three center[d]	−0.012	−0.009	−0.011	−0.004	−0.003
E (cm^{-1})	0.004	0	0	0.159	0.102
E_{SOC} (cm^{-1})[e]	0.001	0	0	0.167	0.113
E_{SS} (cm^{-1})[f]	0.003	0	0	−0.009	−0.011
$\lvert E/D \rvert$	0.003	0	0	0.269	0.288
A (^{55}Mn) (MHz)	−121	−127	−126	−115	−119
g_{iso}	2.011	2.0050	2.0033	2.010	2.0063

[a] The SOC contribution to the total D value. [b] The excitations contributing to the total D_{SOC} value. [c] The SS contribution to the total D value. [d] The n-center contributions to the total D_{SS} value. [e] The SOC contribution to the total E value. [f] The SS contribution to the total E value.

t_{2g} splittings are anisotropic and do not show a similarly pronounced variation with the nature of the halide.

B.3. Calculations of EPR Parameters. The ZFS parameters of the five remaining models have been calculated using spin-unrestricted DFT calculations on the BP86 level on the basis of (a) our recent implementation of the spin−spin contribution to the ***D*** tensor,[4,10d] (b) the Pederson-Khanna formalism for the estimation of the SOC contribution,[7a] and (c) the SOMF operator for the representation of the spin−orbit coupling.[20] The results obtained for the final D values and their breakdown into individual contributions as well as the E/D (and the manganese isotropic hyperfine together with the isotropic g value) are displayed in Table 7.

Non-ZFS Parameters. We note in passing that the isotropic ^{55}Mn hyperfine coupling constants (HFCs) are calculated in the range of −115 to −127 MHz, which is notably smaller in magnitude than that of the experimental HFCs (170−280 MHz)[3], thus confirming the scaling factor of 1.5 previously proposed for the correction of this quantity.[31] As expected for ^{6}S ions, the isotropic g values show rather unspectacular deviations from the free-electron g value. Nevertheless, a significant increase of the isotropic g values is noted from the $\mathbf{M}^{Cl}$ ($g_{iso} = 2.0033$) to $\mathbf{M}^{I}$ ($g_{iso} = 2.011$), which parallels the trend in the SOC constants of the halide ligands, as will be analyzed more completely for the ***D*** tensor below.

Overall *D* Parameter. The D parameters calculated for the various models are in excellent qualitative agreement with the available experimental data on similar molecules. The trends of the variations of D with the nature and arrangement of the halide ligands are correctly reproduced. Furthermore, E/D ratios close to zero were found for the trans series and are consistent with the effective axial symmetry of the electronic structure in these models. By contrast, the E/D ratios of the cis models are almost perfectly in the rhombic limit ($E/D \sim 0.3$), thus agreeing with the distorted geometry found around the Mn^{II} ion.

Orientation of the *D* Tensor. The orientations of the principal axis of the ***D*** tensor are shown in Figure 3 for both the *trans*- and *cis*-$\mathbf{M}^{I}$ models. Comparable results were observed for the Br and Cl models. In *trans*-$\mathbf{M}^{I}$, the axis of the D_{ZZ} tensor is along the X−Mn−X axis, as expected. Concerning *cis*-$\mathbf{M}^{I}$, the $\boldsymbol{D}_{XX}$ tensor component is oriented along the molecular z axis, whereas the two other orientations of ***D*** do not coincide exactly with any of the molecular axes. Indeed, the D_{ZZ} and D_{YY} directions make an angle of 14° with the molecular axes x and y, respectively, both located in the equatorial plane of the octahedron. Accordingly, the easy axis of ***D*** is essentially oriented along a X−Mn−N axis. Note, however, that in the rhombic limit the nature of the easy axis is ambiguous, since even small geometric distortions can lead to a flipping of the eigenvalues of the ***D*** tensor and a different assignment. Thus, in such an arrangement, a much more variable orientation of ***D*** is to be expected. In fact, non-co-incidence of the principal axes of ***D*** with the molecular axes has been observed in two recent single-crystal EPR studies on Mn^{II} complexes.[32]

SS Contributions to *D*. In the case of the models studied here, the dipolar SS interaction contributes up to 0.06 cm^{-1} to D in all models (Table 7). Consequently, this contribution is completely negligible for the heavier halides (Br, I), whereas it becomes comparable to the individual D_{SOC} contribution already present for the $\mathbf{M}^{Cl}$ model(s). In general, we have observed that in many Mn^{II} complexes, the SS contribution must be taken into account to obtain a good correlation between theory and experiment. D_{SS} can be decomposed into n-center contributions ($n = 1-4$). Fortunately, the major portion of D_{SS} originates from the one-center and two-center contributions; for the trans models they are comparable, whereas in the case of the cis models, only the one-center terms notably contribute to D_{SS}.

(31) (a) Kosky, C. A.; Gayda, J.-P.; Gibson, J. F.; Jones, S. F.; Williams, D. J. *Inorg. Chem.* **1982**, *21*, 3173. (b) Carmieli, R.; Manikandan, P.; Epel, B.; Kalb (Gilboa), A. J.; Schnegg, A.; Savitsky, A.; Möbius, K.; Goldfarb, D. *Biochemistry* **2003**, *42*, 7863.

(32) Carmieli, R.; Larsen, T.; Reed, G. H.; Zein, S.; Neese, F.; Goldfarb, D. *J. Am. Chem. Soc.* **2007**, *129*, 4240.

Table 8. Calculated Electronic Parameters D (in cm^{-1}), D_{SOC}, and D_{SS} and the Contributions to the D_{SOC} and D_{SS} Parameters for the $\mathbf{M}^{I}$ and $\mathbf{M}^{Br}$ Models in Three Cases: Z_{eff} with Their Default Values, All Atoms (tot), and Z_{eff} Set to Zero for Either Mn (−Mn) or the Halide (−I, Br)

	trans-$\mathbf{M}^{I}$			*trans*-$\mathbf{M}^{Br}$			*cis*-$\mathbf{M}^{I}$			*cis*-$\mathbf{M}^{Br}$		
	tot	−Mn	−I	tot	−Mn	−Br	tot	−Mn	−I	tot	−Mn	−Br
D^{SOMF} [a]	+1.358			+0.541			+0.590			+0.355		
$D^{Z_{eff}}$ [b]	+1.500	−0.479	+0.103	+0.733	−0.027	+0.073	+0.678	+0.480	+0.042	+0.337	+0.068	+0.029
D_{SS} [c]	+0.047	+0.048	+0.048	+0.041	+0.041	+0.042	+0.023	+0.001	+0.023	+0.020	+0.007	+0.019
one center [d]	+0.033	+0.034	+0.035	+0.007	+0.007	+0.007	+0.035	+0.003	+0.036	+0.020	+0.012	+0.021
two center [d]	+0.026	+0.026	+0.025	+0.047	+0.047	+0.047	−0.008	−0.008	−0.008	+0.003	−0.011	+0.002
three center [d]	−0.012	−0.012	−0.012	−0.013	−0.013	−0.013	−0.004	+0.007	−0.004	−0.003	+0.005	−0.003
D_{SOC} [e]	+1.452	−0.521	+0.054	+0.692	−0.067	+0.032	+0.654	+0.478	+0.019	+0.318	+0.060	+0.009
$\alpha \rightarrow \alpha$ [f]	+7.913	+7.741	+0.005	+0.600	+0.522	+0.003	+2.985	−3.543	+0.002	+0.279	−0.259	+0.001
$\beta \rightarrow \beta$ [f]	+9.895	+9.226	+0.017	+0.833	+0.580	+0.014	+4.290	−5.180	+0.011	+0.457	−0.415	+0.010
$\alpha \rightarrow \beta$ [f]	−9.674	−10.832	+0.035	−0.310	−0.763	+0.017	−4.445	+6.301	+0.009	−0.248	+0.550	+0.001
$\beta \rightarrow \alpha$ [f]	−6.682	−6.656	−0.003	−0.431	−0.406	−0.002	−2.176	+2.900	−0.003	−0.170	+0.184	−0.003

[a] $D^{SOMF}$is related to eqs 3 and 4. [b] $D^{Z_{eff}}$ is related to eq 2. [c]The SS contribution to the total D value. [d] The n-center contributions to the total D_{SS} value. [e] The SOC contribution to the total D value. [f]The contribution of the indicated excitation class to the total D_{SOC} value.

Spin−Orbit Contributions to *D*. At this point, a better understanding of the different contribution to the D_{SOC} part is required. As discussed in more detail elsewhere, four types of excitations have to be considered. In the one-electron approximation, they take the forms noted here: (i) excitation of a spin-down (β) electron from a doubly occupied MO (DOMO) to a SOMO leading to states of the same spin S as that of the ground state ($\beta \rightarrow \beta$); (ii) the excitation of a spin-up (α) electron from a SOMO to a virtual MO (VMO) also giving rise to states of total spin S ($\alpha \rightarrow \alpha$); (iii) excitations between two SOMOs that are accompanied by a spin-flip and giving rise to states of $S' = S - 1$ ($\alpha \rightarrow \beta$); and (iv) "shell-opening" transitions from a DOMO to a VMO leading to states of $S' = S + 1$ ($\beta \rightarrow \alpha$).

Although the four classes of excitations can contribute to the $\boldsymbol{D}$ tensor, ligand-field theory for high-spin d^5 systems focuses on only class iii ($\alpha \rightarrow \beta$). All other contributions would be classified as charge-transfer contributions in ligand-field language and would be discarded as being small for Mn^{II}, since there are usually neither appreciable ligand-to-metal charge transfer nor metal-to-ligand charge transfer states that at least fall in the visible region of the spectrum. However, from Table 7, it can be seen that the magnitudes of the different contributions coming from the four excitations are actually *comparable* and show partially cancelling signs (the pairs $\alpha \rightarrow \alpha$; $\beta \rightarrow \beta$ and $\alpha \rightarrow \beta$; $\beta \rightarrow \alpha$ lead to contributions of opposite sign). The trend in the magnitudes of the individual excitation class contributions parallels the trend in the final D value. However, the individual contributions may exceed the magnitude of the final D value by up to a factor of 4 (for *trans*-$\mathbf{M}^{I}$). These results have two important implications: (a) The calculation of D values in Mn^{II} complexes is a very complicated undertaking since there are five contributions of two-electron nature that are of the same order of magnitude (four from the SOC and one from the SS part) but have partially opposing signs and different physical content. The accurate and balanced calculation of all contributions is clearly a major challenge to quantum chemistry. (b) The ligand-field models of the ZFS in high-spin d^5 complexes cannot be realistic, not even in the case of Mn^{II}, which is a "best-case scenario" owing to the very limited covalent bonding.

Metal versus Ligand Spin−Orbit Coupling Contributions. To assess the relative contributions of the halide SOC to the D value, an additional series of calculations was carried out where the SOMF operator was replaced with the effective nuclear charge SOC model of Koseki et al.[22] (see the Experimental Section). The advantage of this operator (eq 2) over the more rigorous and accurate SOMF approach for the purpose of this section is that it is possible to set Z_A^{eff} for individual atoms to zero, which allows the determination of the contributions of this atom to the D value. In general, there will be one-, two-, and three-center contributions to the SOC matrix elements. These one-center values reflect the local (atomic) SOC—the only contribution taken into account in ligand-field theory. The two-center terms arise from the orbital motion of the electrons situated in the surrounding bonds and on the surrounding atoms around a given nucleus. The (very small) three-center terms arise from orbital motions of electrons in remote bonds around a given nucleus.

The results are collected in Table 8. First of all, we note that the agreement of the results obtained with the SOMF and Z_{eff} representations of the SOC operator are similar for all models. The limited deviations between the two approaches are of no importance for the qualitative discussion below. As expected, comparable D_{SS} contributions have been calculated using both representations, since the Z_{eff} representation only affects the SOC part of D. There are a number of striking observations in studying the SOC contributions to D in Table 8: (a) The contribution of the halide is much larger than the contributions of the metal. (b) The contributions of the metal and the halide are not even nearly additive. (c) $|D_{SOC}|$ is much smaller than its components that cancel, to a large extent. From these observations, it becomes even more evident that models that try to explain the ZFS in these Mn^{II} halide complexes based on ligand-field models that neglect the ligand SOC cannot lead to realistic results. In particular, the nonadditivity of the contributions may appear puzzling at first glance, since in $\boldsymbol{g}$ tensor calculations the SOC contributions are additive in atomic contributions to a good approximation. One possible explanation for this observation would be that multicenter contributions to the SOC matrix elements may be unusually large. These are

Table 9. Analysis of Interference Contributions (BP86/TZVP) to the SOC Part of the *D* Value for an Idealized Octahedral Model of *trans*-$\mathbf{M}^{Br}$ with Mn−N Distances of 2.30 Å and Mn−Br Distances of 2.65 Å (All Values are in cm^{-1})

		$\alpha\rightarrow\alpha$	$\beta\rightarrow\beta$	$\alpha\rightarrow\beta$	$\beta\rightarrow\alpha$	D_{SOC}
full Z_{eff}	D	0.424	0.536	−0.457	−0.340	0.163
	$D_{xx}=D_{yy}$	−29.147	−29.361	29.885	28.861	0.238
	D_{zz}	−28.723	−28.825	29.429	28.520	0.401
$Z_{eff}(Mn)=0$	D	0.398	0.444	−0.510	−0.337	−0.005
	$D_{xx}=D_{yy}$	−26.827	−27.094	27.291	26.641	0.011
	D_{zz}	−26.430	−26.651	26.783	26.304	0.005
$Z_{eff}(Br)=0$	D	0.002	0.007	0.003	−0.003	0.009
	$D_{xx}=D_{yy}$	−2.315	−2.218	2.646	2.322	0.344
	D_{zz}	−2.313	−2.211	2.649	2.229	0.354
interference	D	0.033	0.085	0.050	0.000	0.168

represented by integrals of the form $(\varphi_A|SO(B)|\varphi_{'A})$, $(\varphi_A|SO(A)|\varphi_B)$, and $(\varphi_A|SO(B)|\varphi_C)$, which represent "point charge", "bond", and "three-center" contributions, respectively (*A*, *B*, and *C* refer to atomic centers and SO(*A*) is the part of the SOC operator that is centered on atom *A*). This possibility was numerically investigated by setting all of the multicenter integrals to zero, which is easily done in the *ORCA* code. However, the numbers obtained in these calculations (not shown) are essentially identical to those collected in Table 8. Thus, the conclusion is that the nonadditivity arises from one-center terms. Although it appears contradictory on first glance that "multicenter effects arise from one-center contributions", the answer lies in two facts: (a) the $\boldsymbol{D}$ tensor—unlike the $\boldsymbol{g}$ tensor—is quadratic in the SOC, and (b) the *D* value $= D_{zz} - (D_{xx} + D_{yy})/2$ arises as a difference between the principal values of the $\boldsymbol{D}$ tensor.

Thus, the evaluation of eq 3 integrals of the form $\langle\psi_i^\sigma|h_K^{SOC}|\psi_a^{\sigma\prime}\rangle\langle\psi_a^{\sigma\prime}|h_L^{SOC}|\psi_i^\sigma\rangle$ must be evaluated. For simplicity, let us study an occupied/virtual pair of the simplified forms $\gamma|\varphi_d^{Mn}\rangle + \sqrt{1-\gamma^2}|\varphi_p^X\rangle$ and $\delta|\varphi_{d'}^{Mn}\rangle + \sqrt{1-\delta^2}|\varphi_{p'}^X\rangle$ where d,d' and p,p' represent metal d and ligand p orbitals, respectively, and γ and δ are the mixing coefficients that are related to metal−ligand covalency. This gives products of the form

$$\langle\psi_i^\sigma|h_K^{SOC}|\psi_a^{\sigma\prime}\rangle\langle\psi_a^{\sigma\prime}|h_L^{SOC}|\psi_i^\sigma\rangle \approx \gamma^2\delta^2\zeta_{Mn}^2|L_{dd'}|^2 + (1-\gamma^2)(1-\delta^2)\zeta_X^2|L_{pp'}|^2 + 2\gamma\delta\sqrt{1-\gamma^2}\sqrt{1-\delta^2}\,\zeta_{Mn}\zeta_X Re(L_{dd'}L_{pp'}) \quad (6)$$

where ζ_{Mn} and ζ_X are the SOC constants of the Mn and halide and $L_{dd'}$, $L_{pp'}$ are one-center angular momentum matrix elements.[5b] From this expression, it becomes evident how the cross terms arise from a product of one-center terms. They will maximize for high covalencies where the mixing of metal and ligand orbitals becomes significant, which is not the case for Mn^{II}, which has very limited covalency. Second, the expression shows that for bonding/antibonding pairs, the contribution to the matrix element pair will be negative, whereas for bonding/bonding or antibonding/antibonding pairs, the cross terms will enhance the matrix element product.

To see how the cross terms contribute to the actual *D* value, some realistic numbers that were obtained for an even more simplified model of *trans*-$\mathbf{M}^{Br}$ are quoted (Table 9). Here, the *D* value is only $+0.163\ cm^{-1}$ due to the artificially high pseudo-octahedral symmetry. The interference contribution to this value is +0.168 and thus accounts for essentially the entire *D* value. This arises from an extensive cancellation of much larger individual contributions from the different excitation classes (last column of Table 9). The net effect is to make the individual Mn and Br contributions negligible despite the fact that different excitation classes contribute as much as $\pm0.5\ cm^{-1}$ and the absolute values of the $\boldsymbol{D}$ tensor elements are as large as $\pm30\ cm^{-1}$. Noticeably, by far the larger contribution to the $+30\ cm^{-1}$ value comes from the bromine SOC, which clearly dominates the Mn SOC. In fact, the Mn−SOC contribution is quite close to zero, which shows that the effective electronic symmetry around the Mn center is close to cubic and the anisotropy in the magnetic interaction is essentially caused by the halide SOC through the Mn/Br interference contributions.

Discussion

In this work, a detailed combined experimental and quantum chemical analysis of the zero-field splitting in a series of Mn^{II} dihalide complexes has been performed.

We determined both the structural and electronic properties of a series of dihalide mononuclear Mn^{II} complexes in a cis configuration. The *D* values obtained for **1**−**3** are very close to those of the phen series, confirming the important effect of the configuration of the two halides on *D* in six-coordinate complexes. Indeed, the magnitude of *D* is comparable for complexes containing the same halide (X = I, Br, Cl) in the case of four-, five-, and *trans*-$(X)_2$ six-coordinate complexes (Table 3), whereas the *cis*-$(X)_2$ six-coordinate ones present significantly lower *D* values (a decrease by a factor of 2). From Table 3, it appears that the *E*/*D* ratio depends predominantly on the nature of the neutral ligand. With monodentate ligands such as pyr, the systems are quasi-axial ($E/D = 0$), whereas with bi-, tri-, or tetradentate ligands, the steric constraints cause an increase in the *E*/*D* ratio for the six-coordinate complexes. The *E*/*D* ratios for **1**−**3** lie between 0.15 and 0.21, reflecting the distortions observed in their X-ray structure.

The experimental ZFS values were subjected to a detailed theoretical investigation, which has purposely focused on simplified small models that served to disentangle the various contributions to the *D* value. In this work, we have focused on the physical origin of the *D* value and avoided theoretical details as much as possible. A complete calibration study of a much larger series of Mn^{II} complexes will be presented elsewhere, where the impact of all relevant technical details of the calculational methodology will be studied to rigorously assess the achievable accuracy of the predictions. This is of obvious importance for future applications to low-symmetry Mn^{II} sites[32] of perhaps even unknown structure. Nevertheless, the overall agreement between theory and experiment achieved in this work is already acceptable. The calculations properly reproduce all experimentally observed trends in the ZFS values. Thus, *D* increases considerably for the heavier halides and is a factor of 2 smaller for the cis compared to the trans arrangement. A closer analysis of the calculated results reveals that the origin of *D* in these Mn^{II} complexes

is highly complex, which precludes any ligand-field-type analysis from providing realistic conclusions. The main results of the analysis are: (a) Spin−spin coupling contributions to the ***D*** tensor are non-negligible for the lighter halides (F, Cl) but become insignificant for the heavier halides. (b) No single excitation class (spin-conserving versus spin-flip) dominates the ***D*** tensor, and extensive cancellation between contributions of different signs occurs. (c) The halide SOC dominates the *D* value in these complexes but in a very complex way: whereas only genuine one-center contributions are significant, the dominant contributions arises from interference between the metal and halide SOC contributions, which are proportional to $\zeta_{Mn}\zeta_X$ (X = Cl, Br, I). This is possible due to two reasons: (1) The ***D*** tensor is quadratic in the SOC rather than linear; thus, a similar interference does not occur in ***g***-tensor calculations where the ***g*** tensor can, to a good approximation, be decomposed into single atom contributions. (2) The observable *D* value is a difference between the principal values of the ***D*** tensor that may be 1−2 orders of magnitude larger than the *D* value itself.

This admittedly somewhat elaborate analysis puts the task that the quantum chemical methods face into clear perspective: To predict accurate *D* values for Mn^{II} complexes, it is necessary to calculate small differences between large contributions of varying sign of different physical origin to a high precision. This is clearly a major challenge that will require significant future efforts before systematically high accuracy can be obtained for this property. When viewed from this angle, the reasonable success of the relatively simple calculations pursued in this work is surprising and to some extent also encouraging.

Acknowledgment. We thank Dr. H. Weihe from the chemistry department of The University of Copenhagen, Denmark, for the simulation software. F.N. gratefully acknowledges the financial support of this work by the Deutsche Forschungsgemeinschaft (priority program 1137, "Molecular Magnetism", and special research unit SFB 663, "Molecular Response to Electronic Excitation") and by the German−Israeli Foundation (Grant I * 746-137.9/2002). S.Z. thanks the Alexander von Humboldt Foundation for a postdoctoral fellowship.

Supporting Information Available: CIF files of the X-ray structures of complexes **1**−**3**, experimental HF-EPR spectra of compounds **1**−**3** at low temperature, and a representation of the eg orbitals of the *trans*- and *cis*-$[Mn(NH_3)_4I_2]$ models. This material is available free of charge via the Internet at http://pubs.acs.org.

IC062384L